Structural Engineering and Mechanics, *Vol. 95, No. 6 (2025) 507-520*
https://doi.org/10.12989/sem.2025.95.6.507

Transformable underwater docking mechanism based on origami-inspired deployable and bistable structures

Gagyeong Park[1†], Ki-Hoon Lee[1†], Sung-Jin Lee[1], Seongjun Lee[1],
Minseop Lee[2], Daegyoum Kim[2] and Dae-Young Lee[*1]

[1]*Department of Aerospace Engineering, Korea Advanced Institute of Science and Technology (KAIST), Daejeon, 34141, Republic of Korea*
[2]*Department of Mechanical Engineering, Korea Advanced Institute of Science and Technology (KAIST), Daejeon, 34141, Republic of Korea*

(*Received August 4, 2025, Revised August 17, 2025, Accepted August 17, 2025*)

Abstract. The increasing deployment of autonomous systems, such as autonomous underwater vehicles (AUVs), highlights a critical need for robust and efficient recovery mechanisms. A significant challenge in extended autonomous operations is the limited onboard battery capacity, which necessitates reliable docking solutions. This paper presents a transformable underwater docking mechanism based on origami-inspired deployable and bistable structures, which can be mounted on a submarine. The proposed docking station system is divided into two components, which are the deployable funnel, and the landing station, respectively. The deployable funnel and landing station employe the Sarrus linkage and bistable structure, respectively. Additionally, the applied structures help reduce the burden on system control, enabling the use of a minimal number of actuators. The grasping forces of both components are analyzed, and the structural stability is simulated. The performance of the proposed mechanism is verified by conducting five underwater docking experiments in a circulation water tunnel with a free-stream velocity of 0.6 m/s.

Keywords: autonomous underwater vehicle; bistable structure; origami; Sarrus linkage; transformable mechanism; underwater docking

1. Introduction

Origami-inspired structural designs have emerged as versatile solutions to address various mechanical and operational challenges across engineering disciplines (Guevara-Corzo *et al.* 2022, Hwang *et al.* 2025, Misseroni *et al.* 2024). Their inherent capability to transition from compact states into expanded functional configurations significantly enhances system adaptability and spatial efficiency (Park *et al.* 2025, Kim *et al.* 2025, Cha *et al.* 2024). One promising area for applying these origami-inspired structures is docking systems for autonomous platforms. Docking applications require precise spatial alignment and robustness against environmental disturbances. Deployable origami mechanisms effectively address these challenges by offering large capture envelopes, thereby easing alignment precision requirements. Such structural advantages are particularly beneficial for autonomous underwater vehicles (AUVs), whose mission durations and exploration ranges are severely constrained by limited battery capacities, underscoring the critical importance of efficient underwater docking systems that enable reliable energy replenishment and data transfer (Esteba *et al.* 2024).

Various underwater docking systems have been studied, primarily involving stationary structures featuring funnel-like guides for charging and data transmission (Guo *et al.* 2024a). Although these stationary docking systems are relatively simple in their design, they often exhibit limited adaptability to dynamic environmental conditions, restricting their operational versatility and exploration range (Zhang *et al.* 2017). Additionally, their fixed locations necessitate considerable time and resources for installation and retrieval, hindering extensive area exploration. Alternatively, free-floating funnel-like docking systems, typically towed by mother ships, have been explored (Martin *et al.* 2016, Lin *et al.* 2022, Guo *et al.* 2024b). However, their applicability remains constrained due to limited mission flexibility and economic impracticality for deep-sea operations.

Docking systems mounted on mobile submarines present a more promising alternative for enhancing mission flexibility and operational range. Prior research has explored various docking systems designed for direct AUV recovery from moving submarines or larger vehicles. For instance, a casing-mounted hanger (CMH) docking structure attached at the rear of a submarine mast has been proposed (Fedor 2009). However, this approach demands substantial mounting space, negatively affecting submarine dynamics, structural stability, increasing operational noise, and reducing energy efficiency due to additional flow resistance. Another method involves a robotic arm for direct AUV docking into a submarine's side torpedo tube (Fedor 2009), though this method faces challenges such as significant system weight (~2000 kg) and operational complexity requiring precise manual control. Additionally,

*Corresponding author, Professor
E-mail: ae_dylee@kaist.ac.kr
†These authors contributed equally to this work.

http://www.techno-press.com/journals/semandsubpage=7
ISSN: 1225-4568 (Print), 1598-6217 (Online)

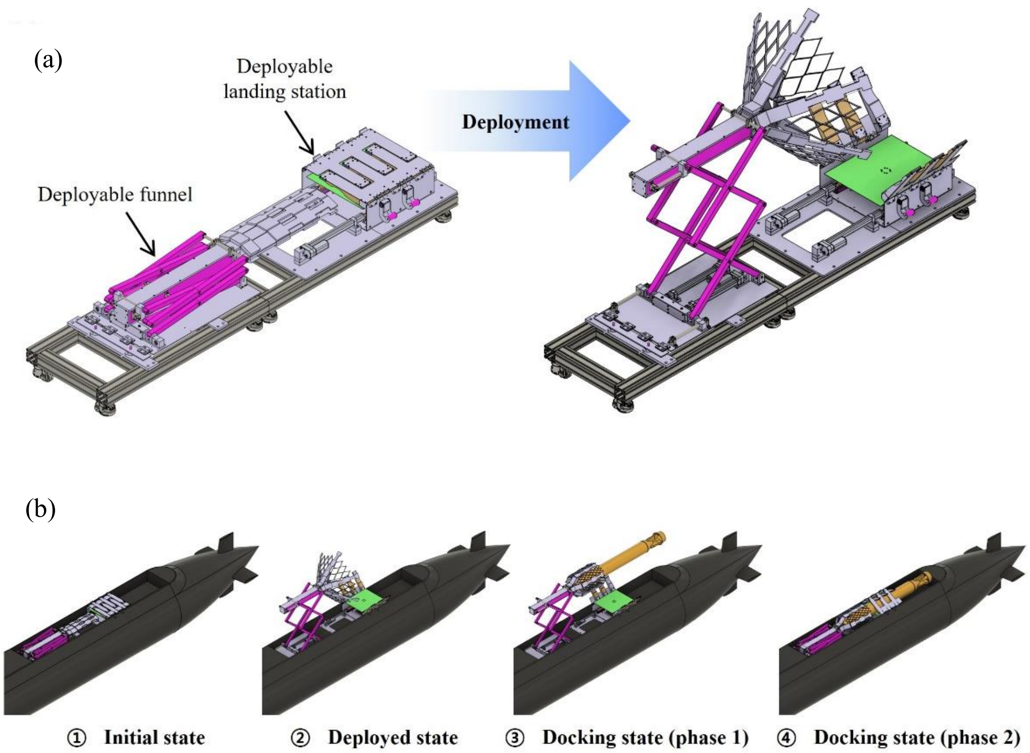

Fig. 1 (a) Transformable underwater docking mechanism in the stowed and the deployed state. (b) Docking process of the proposed system

a recent study proposed a mobile docking station using a fork-pole mechanism (Zhang *et al*. 2023), but this method provides limited grasping force necessary for reliable charging and data transmission. Docking mechanisms inspired by origami (Tian *et al.* 2024) and octopus tentacles (Li *et al.* 2025) have also been proposed, showing promising conceptual advantages, though further verification under realistic underwater conditions would strengthen their applicability. Continued development of these approaches has the potential to overcome existing alignment challenges and enhance their practical deployment.

In this paper, we propose a transformable underwater docking mechanism employing dual-deployable, and bistable origami-inspired structures. The mechanism folds compactly, minimizing structural load and hydrodynamic impact on the host submarine. As illustrated in Fig. 1(a), the docking mechanism comprises two main components: a deployable funnel for initial capture and guidance of the AUV, and a deployable landing station designed for secure docking and stabilization on the host submarine, as depicted in Fig. 1(b).

This separation of grasping and stabilizing functions allows each component to be designed independently with distinct objectives, representing a departure from conventional single-structure docking systems. The grasping function prioritizes maximizing the guidance envelope and accommodating positioning uncertainties. In contrast, the stabilizing function focuses on restricting the movement of the AUV and reducing impact with the host submarine. In other words, the deployable funnel emphasizes expandability, while the landing station requires structural rigidity and secure grasping force. By separating the functions, the proposed system eliminates the need to compromise between these conflicting requirements.

The funnel utilizes a modified Sarrus linkage origami structure, allowing dual-stage deployment with a single actuator, thereby ensuring operational simplicity and robustness. Subsequently, the landing station passively secures the AUV through a structurally bistable capture mechanism, further reducing complexity in control requirements. Overall, the compact design (folded height of 0.2 m) and simplified single-degree-of-freedom actuation significantly enhance submarine mobility and efficiency. The feasibility and effectiveness of the proposed system have been validated through experiments conducted in a circulation tank environment.

2. Design of deployable underwater docking station

2.1 Design of deployable funnel

In the deep sea, determining the position of the AUV accurately is a significant challenge, necessitating a wide guidance area for successful docking. Despite this requirement for a wide guidance area, the docking station needs to be compactly stowed when not in operation with high system reliability. Therefore, a modified Sarrus linkage origami structure is proposed to achieve the requirement with a single actuator.

The Sarrus linkage is a structure that converts linear motion into rotational motion (Waldron *et al.* 2016, Koetsier *et al.* 2012). Fig. 2(a) shows the actuation concept

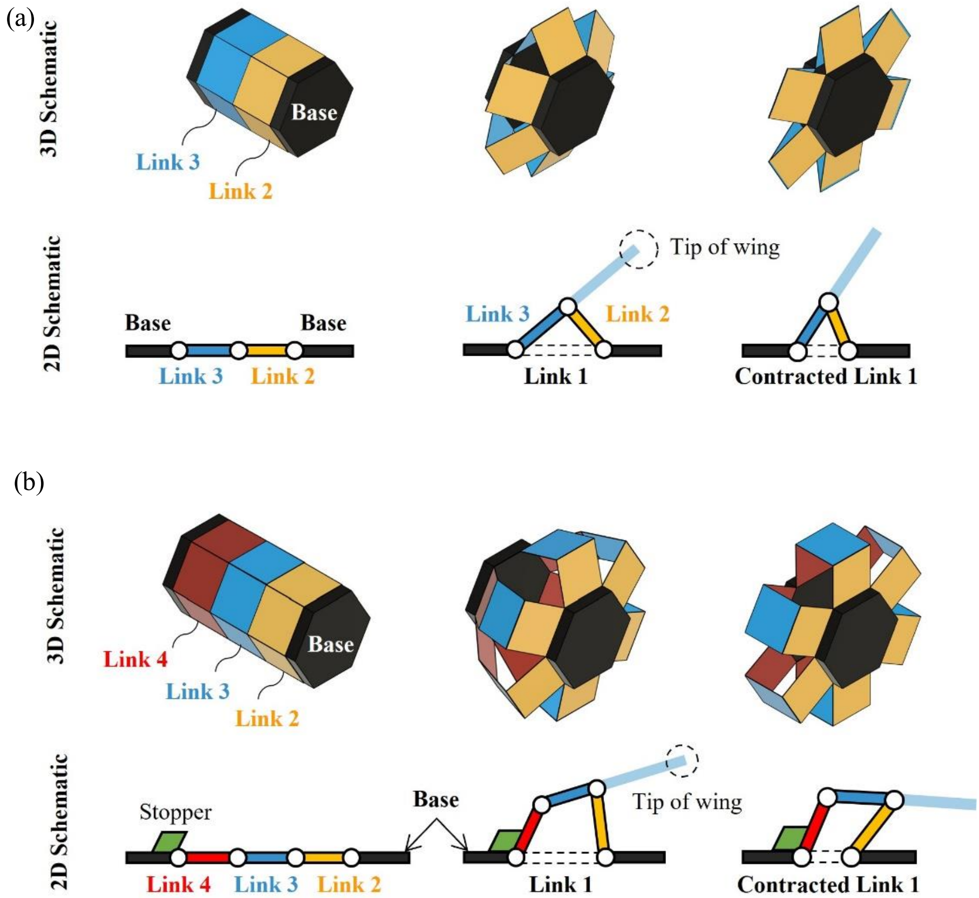

Fig. 2 (a) The concept of the six-sided Sarrus linkage in 3D schematic and 2D schematic. (b) The concept of the modified six-sided Sarrus linkage in 3D schematic and 2D schematic

of the Sarrus linkage in 3D and 2D schematics. The linear motion of the top and bottom bases, corresponding to the contraction of Link 1, is mechanically converted into the rotational motion of six panels, each composed of a pair of linked elements. The rotating faces maintain the parallel alignment of both bases, constraining their motion to a single degree of freedom (1-DOF). Additionally, the wide guide area is achieved by elongating Link 3 of each face, which is referred to as a wing. However, the conventional Sarrus linkage is difficult to capture the AUV tightly because the area of the guide cannot shrink sufficiently even though the length of Link 3 is longer than Link 2. This problem is solved by adding an additional link to each face as illustrated in Fig. 2(b). However, although the guide area can be reduced for AUV docking due to added Link 4, the increased DOF results in a drawback where the system does not reach zero DOF even when the length of Link 1 is fixed. To address the disadvantage, the joints of the modified Sarrus linkage are designed using spring hinges and stoppers are utilized to ensure that the mechanism maintains approximately zero DOF even when the length of Link 1 is fixed, which is analyzed in Section 3. Consequently, the modified Sarrus linkage structure allows the retraction of a single linear actuator to directly apply force to the AUV. Thus, the six-sided modified Sarrus linkage structure is employed to design the deployable funnel with adjusted link lengths.

Moreover, the top and bottom bases of the deployable funnel are divided into three rectangular components, which can enhance storage efficiency by folding the bases. Thus, the deployable funnel features the dual-stage deployment: the deployment of the bases in the first stage, followed by the deployment of the wings in the second stage. The detailed deployable funnel structure is illustrated in Fig. 3 along with a concept diagram based on origami. The green links compose the top and bottom bases of the modified Sarrus linkage structure, and they can be deployed by retracting the linear actuator. From the initial state, the structure transforms into hexagonal prism as shown in the front view of the first stage of the deployed state. Further retraction leads to the second stage of the deployed state, in which the structure is prepared for docking. The area of the funnel becomes largest in the second stage of the deployed state, enabling the AUV to be guided reliably. An additional retraction facilitates the capture of the AUV by generating sufficient grasping force. Conversely, extension of the linear actuator enables the release of the AUV and the return to the initial state. This bidirectional motion allows the mechanism to alternate between grasping and releasing states.

2.2 Design of deployable landing station

One significant challenge encountered by host

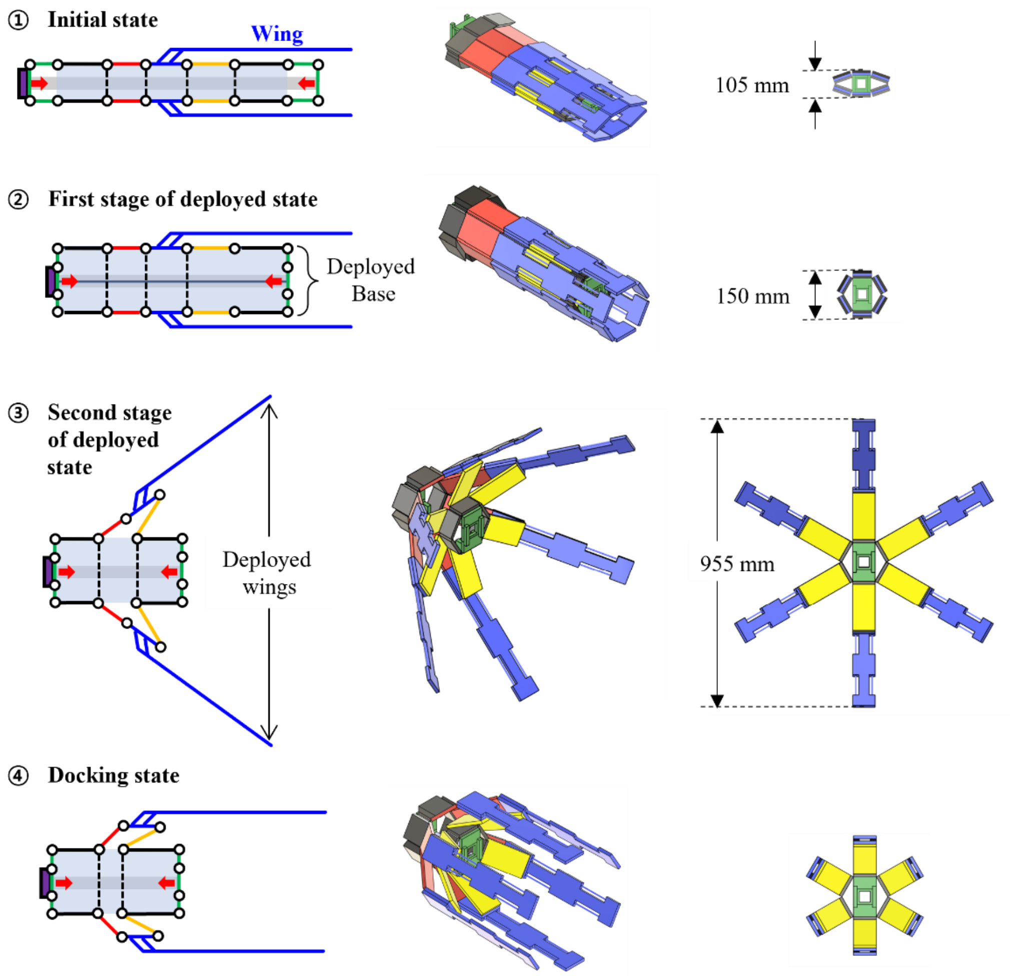

Fig. 3 Concept diagram based on origami (left) and detailed design of the deployable funnel in isometric view (middle) and in front view (right)

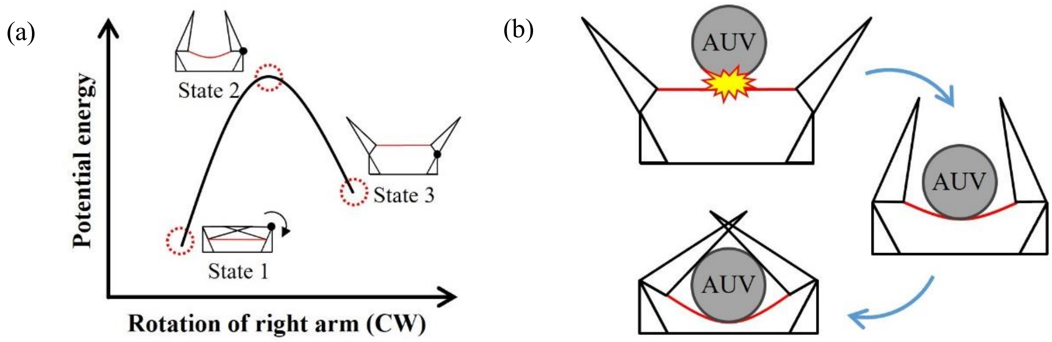

Fig. 4 (a) Potential energy profile of the deployable landing station based on bistable structure. (b) Passive docking process for AUV recovery

submarines during underwater operations involving autonomous underwater vehicle (AUV) recovery is the potential risk of collision, which can lead to irreversible damage, particularly in deep-sea environments. To address this challenge, we propose a bistable structural mechanism capable of mitigating impact forces and securely capturing the AUV without the need for supplementary sensors.

The bistable structure has two different stable states. It can remain in both stable states without continuous energy input, while the transition between these states requires external energy to overcome the potential energy barrier separating them (Morris 1992, Wu *et al.* 2024). In the proposed mechanism, the flexible landing plate can store potential energy through elastic deformation by the rotation of the arms. The conceptual diagram and potential energy profile are shown in Fig. 4(a). State 1 and State 3 are the initial state and the deployed state, respectively, which store the minimum potential energy. State 2 is an unstable state where the landing plate buckles by rotating arms and stores the maximum potential energy.

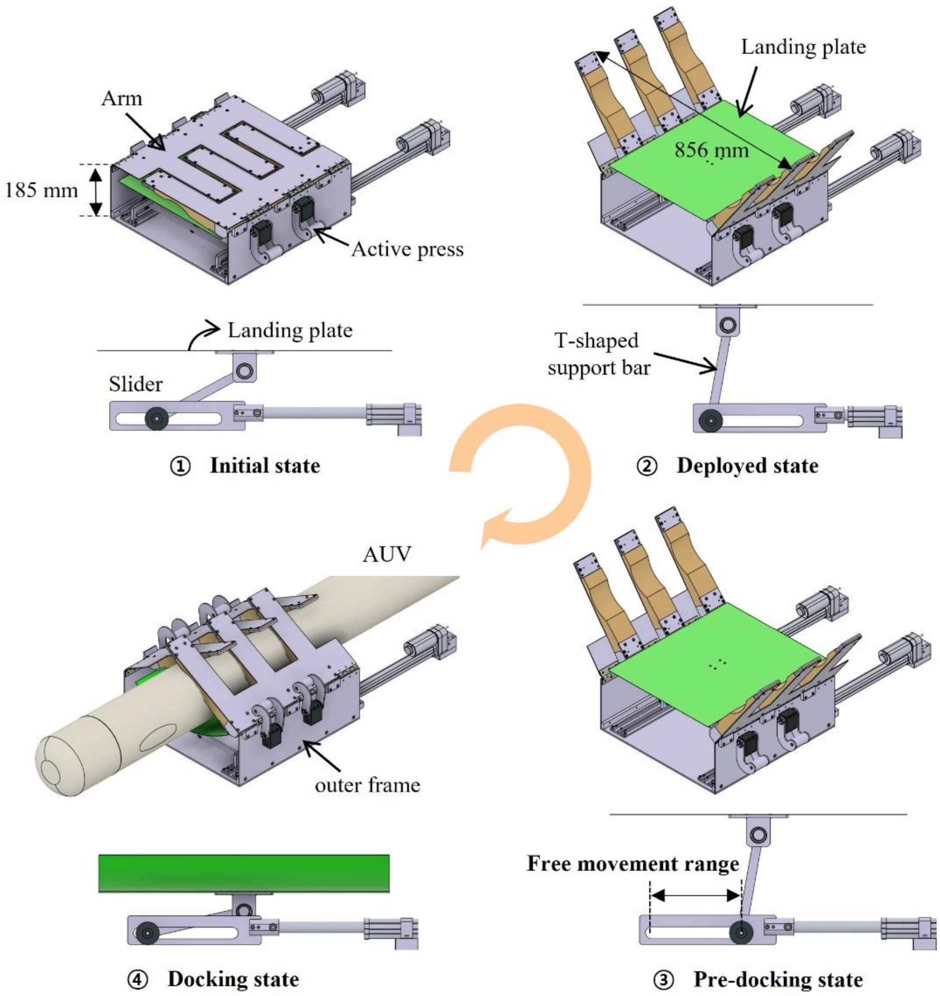

Fig. 5 Detailed actuation with isometric views of the entire mechanism and side views of the interior structures

This mechanism basically requires an external force to enable state transitions. These transitions are required four times during docking cycle: preparing docking (state 1→ state 3), AUV docking (state 3→state 1), AUV relaunching (state 1→state 3), and returning to the initial state (state 3 →state 1), which can be simply achieved by using actuators. However, manual actuator control is difficult under limited visibility, and even automatic control via sensors can increase system complexity, reducing system stability. Consequently, a passive operational mode is necessary for AUV docking moment as shown in Fig. 4(b), which is addressed by providing a range of free movement in the pre-docking state.

The actuation of the landing station depends on the positions of the sliders and the T-shaped bar which is connected at the center of the landing plate as shown in Fig. 5. The horizontal motions of the sliders, which are generated by linear actuators, are converted into the vertical motion of the landing plate, thereby functioning to rotate the two arms simultaneously. Firstly, the deployable landing station rotates the arms by retracting the linear actuators from the initial state to the deployed state. Subsequently, the linear actuators push the slider to reach the pre-docking state. In other words, once the deployable landing station is ready for docking, the T-shaped support bar gains a range of unrestricted movement along the rail, which is equal to the length of the slotted hole of the slider. Therefore, the AUV can be docked passively without any sensors and actuators. In the docking state, the AUV is secured by the restoring force of the flexible landing plate. Additionally, the active presses with servomotors are connected to the arms by waterproof strips, which assist in opening the arms and securing the AUV. So, the active presses can improve reliability of the bistable structure.

3. Analysis of deployable underwater docking station

3.1 Kinematics of deployable funnel

The kinematic representation of the deployable funnel is shown in Fig. 6(a). The constraint conditions of the four-bar linkage, which determine the position of each link, are defined

$$L_4 cos\theta_1 + L_3 \cos(\theta_1 - \theta_4) = L_1 - L_2 cos\theta_2 \quad (1)$$

$$L_4 sin\theta_1 + L_3 \sin(\theta_1 - \theta_4) = L_2 sin\theta_2 \quad (2)$$

$$\theta_1 - \theta_4 = \theta_3 - \theta_2 \quad (3)$$

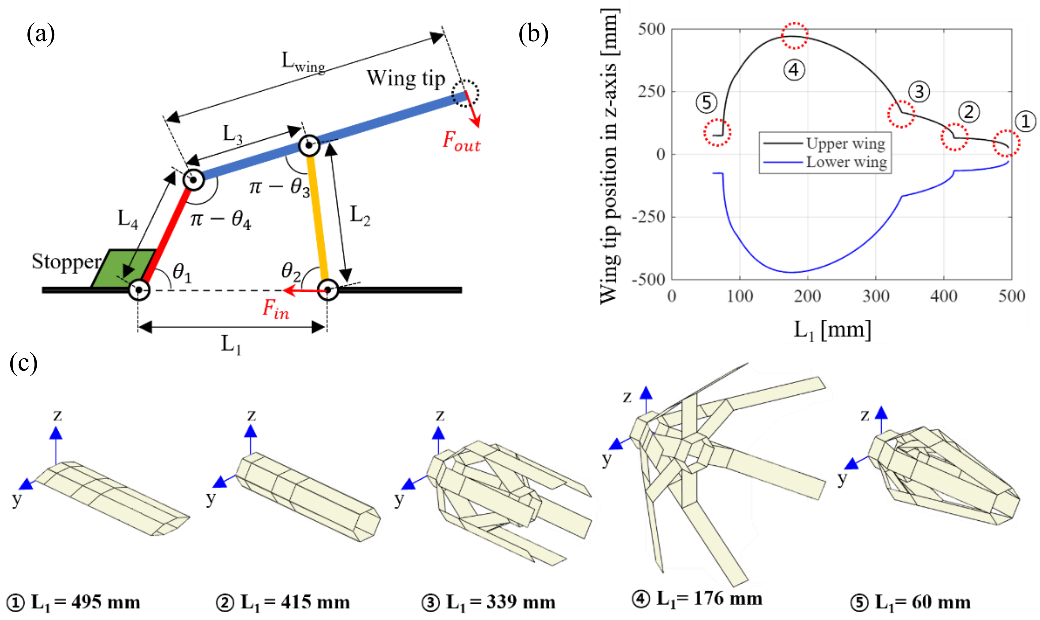

Fig. 6 (a) Kinematic representation of a trap wing (b) Wing tip position in z-axis depending on L_1 (c) Transformation of the funnel mechanism at each point in (b)

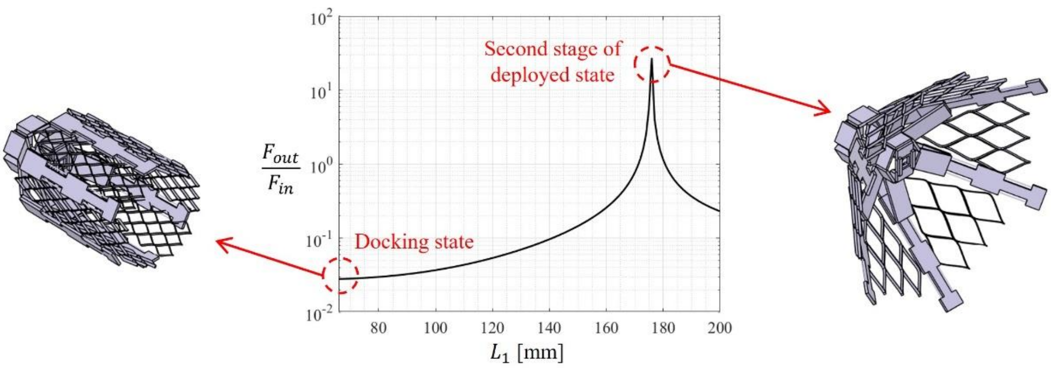

Fig. 7 The force efficiency, F_{out}/F_{in}, depending on L_1

Therefore, a unique combination of hinge angles can be determined by solving the optimization problem that minimizes the value of potential energy of the system, V, while satisfying the constraint conditions, Eqs. (1)-(3). The DOF of the linkage of the deployable funnel is required to be zero for stable grasping force when the length of Link 1 is determined by the linear actuator. However, it is difficult to fix the exact angle of the joints using only the spring hinges. A spring hinge provides restoring torque at a specific angle, but it does not serve as a locking mechanism. Under substantial external loads, such as sudden movement of the AUV, the mechanism is prone to losing its stability. Therefore, a stopper is installed behind the Link 4 (red link) as shown in Fig. 6, while the spring hinge associated with θ_1 exerts a torque which tends to increase its value. Then, the stopper can constrain θ_1, locking the mechanism effectively with nearly zero degrees of freedom. Fig. 6(b) represents the wing tip position in z-axis depending on L_1 and Fig. 6(c) shows deploying motion of the deployable funnel, assuming zero thickness. Considering the tip of the uppermost wing as a reference point, the wing tip height decreases after the second stage of the deployed state, allowing the AUV with a radius of 100 mm to be securely held.

3.2 Grasping force of deployable funnel

The deployable funnel needs to generate sufficient grasping force in the docking state, and the rotating wings serve a critical role. The AUV's movement by water flow induces change of the spring hinges' angle, increasing the funnel's potential energy. Then, the restoring force is generated, which functions as a grasping force in each state of the deployable funnel. The restoring force can be evaluated by calculating the efficiency with which the force of the linear actuator is converted to the force of the wing's tip. The efficiency between the force by the linear actuator, F_{in}, and the force applied to the AUV by the wing, F_{out}, can be obtained by using the principle of virtual work

$$|\delta W_{out}| = |\delta W_{in}| \tag{4}$$

$$\delta W_{in} = F_{in}\,\delta L_1 \tag{5}$$

$$\delta W_{out} = F_{out} L_{wing} \delta\theta_4 \tag{6}$$

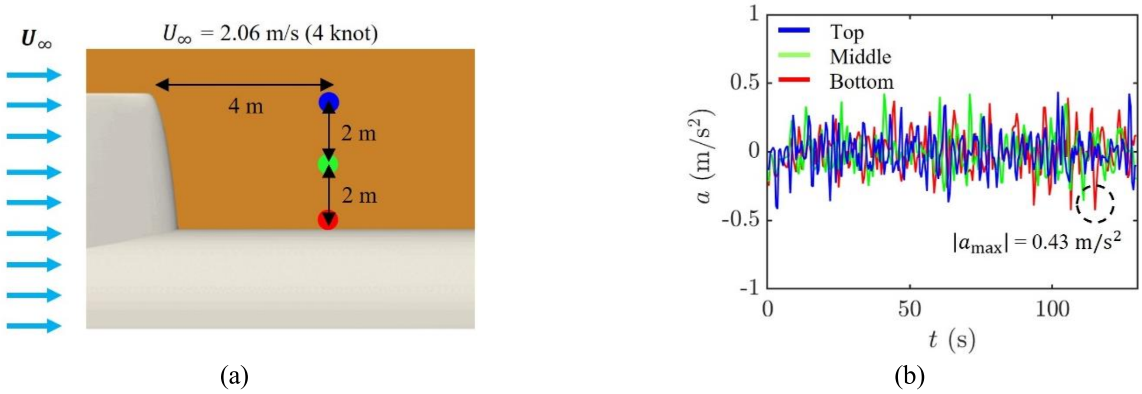

Fig. 8 (a) CFD simulation setup with three acquisition points to obtain a_{max} (b) The result of the simulation which shows a_{max}

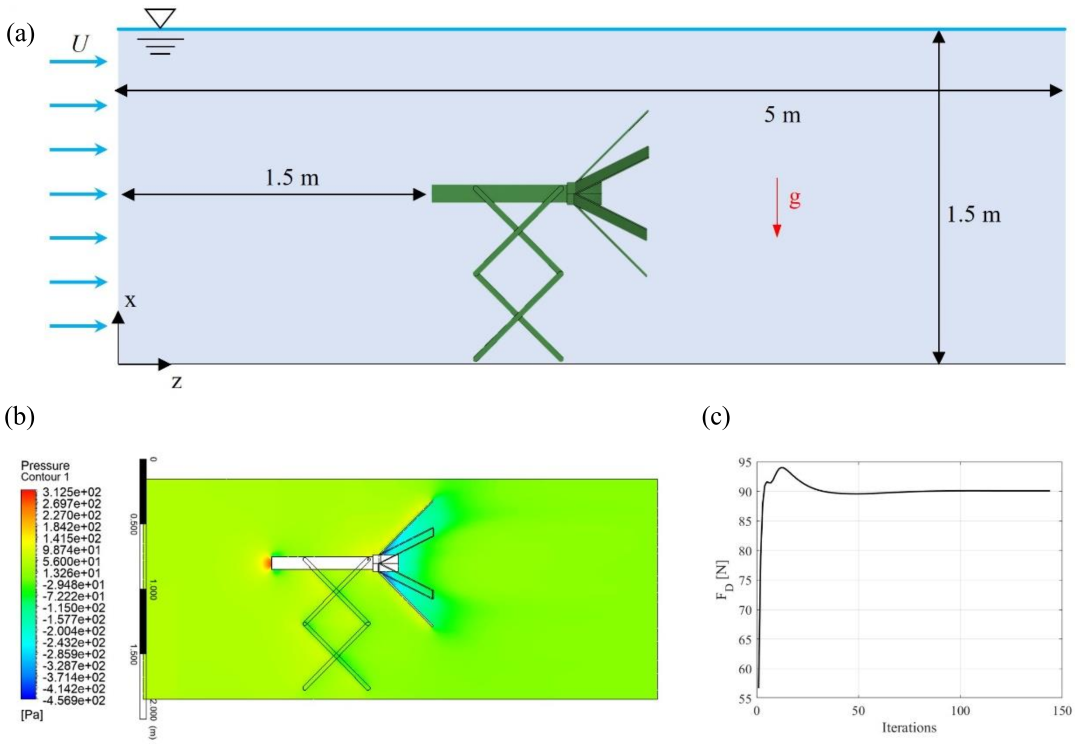

Fig. 9 (a) Configuration for CFD simulation (b) The pressure contour applied on the deployed funnel at the *z*-*x* plane where *y*=0 m (c) The converged simulation result of the drag force applied to the deployed funnel

where δW_{in} and δW_{out} are the work done by the linear actuator, and the wing, respectively, when the linear actuator retracts by δL_1. The total virtual work for the forces by the linear actuator and the wing is zero in equilibrium, which makes δW_{out} and δW_{in} can be considered equal. Then, the force efficiency calculated by Eq. (7) and the force efficiency depending on L_1 is shown in Fig. 7 where L_2, L_3, L_4, and L_{wing} are 170 mm, 100 mm, 145 mm, 450 mm respectively, which are the dimensions of the prototype considering the size of circulation water tunnel for the underwater experiment.

$$\frac{F_{out}}{F_{in}} = \frac{\delta L_1}{L_{wing}(\delta\theta_1 - \delta\theta_4)} \tag{7}$$

In the docking state where $L_1 = 66$ mm, the deployable funnel has the lowest efficiency of 2.8%. This result is used to determine whether the deployable funnel can achieve sufficient grasping force.

When the submarine is in operation, wake flow is generated at the rear of the mast, so the required grasping force needs to be calculated. The unsteady wake flow was analyzed using computational fluid dynamics (CFD) simulation using the commercial tool, Ansys Fluent, and the analysis domain was confined to the wake region to reduce calculation time. The 3D model of the submarine is simplified, and the three acquisition points for velocity and pressure data are illustrated in Fig. 8(a). The free-stream velocity was set to be U_∞=2.06 m/s, which is the velocity of the submarine, and the simulation was conducted based on a transient turbulence model (SST $k-\omega$). The relationship between depth and acceleration was investigated by collecting acceleration data from three different points.

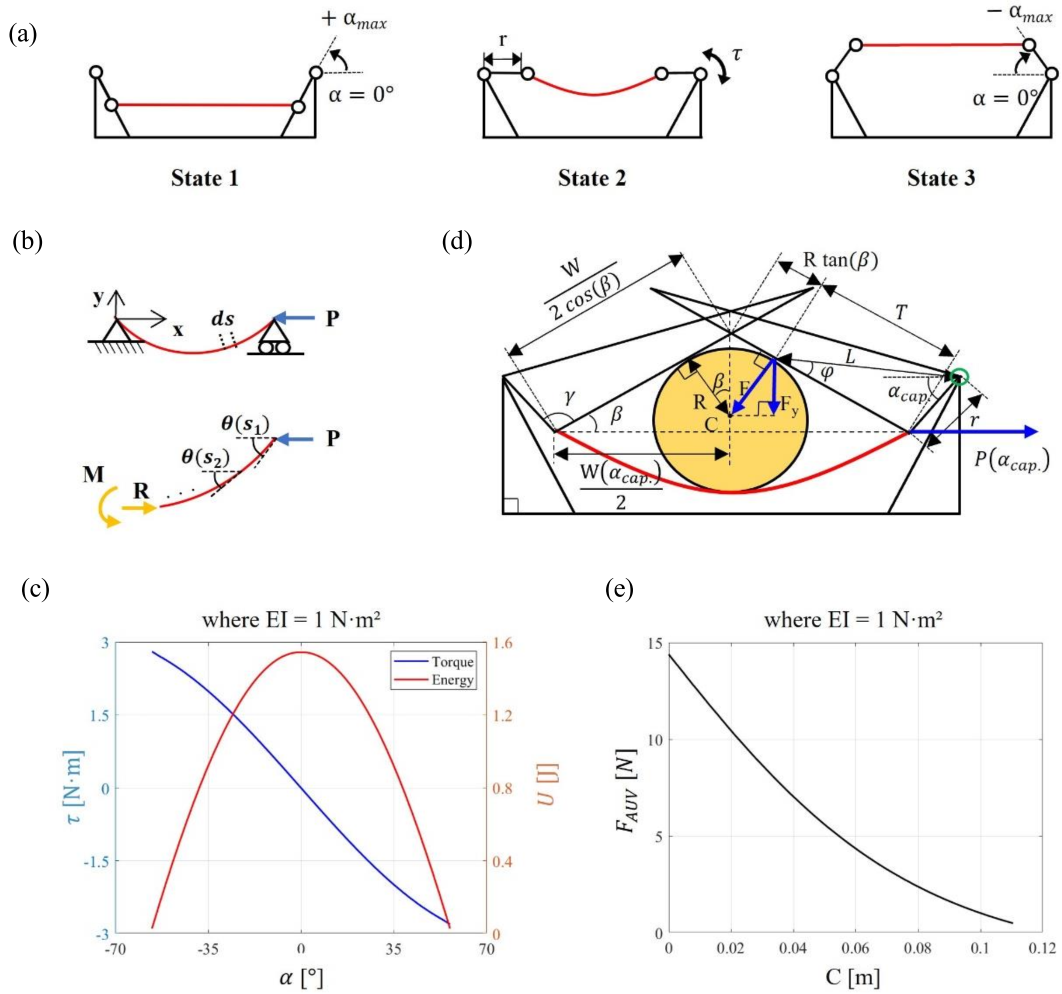

Fig. 10 (a) Concept of the bistable structure of the deployable landing station without arms (b) Free-body diagram of the landing plate (up). The moment and reaction force at a certain point $\boldsymbol{s}$ (down) (c) The torque, τ, and stored energy, U, depending on the rotation angle of the arm, α (d) The dimension necessary for the calculation of the applied force (e) The force that is applied to AUV by the arms, F_{AUV}, depending on the location of the center of the AUV, C

Consequently, the maximum acceleration was determined based on the red-colored graph because the acceleration at the docking area is important. As shown in Fig. 8(b), the maximum acceleration of the AUV movement, a_{max}, is 0.43 m/s^2, which influences the motion of the AUV. Assuming a neutrally buoyant AUV with a diameter of 200 mm and a length of 2500 mm exerts force on the funnel at a_{max}, the required maximum linear actuator force, F_a, can be obtained

$$F_a = m\, a_{max} \frac{F_{in}}{F_{out}}\bigg|_{L_1=66\,mm} = 1206.07\,N \tag{8}$$

where m is the mass of the neutrally buoyant AUV. Therefore, PA-10 linear actuator with a 24-inch stroke from Progressive Automations that has a static force of 2001.70 N was selected for the prototype.

3.3 Drag force by water flow on deployed funnel

The effect of the water flow on the deployed funnel is evaluated through CFD simulation using the commercial tool, Ansys Fluent, to figure out that the deployed funnel can withstand the drag force. Given the conditions of the circulation water tunnel, the free-stream velocity, U, is 0.6 m/s with fluid density, ρ, of 998 kg/m³, and dynamic viscosity of 1.003 mPa·s at 20℃. The volume of the assessment area is $2 \times 5 \times 1.5$ m^3, and the configuration is shown in Fig. 9(a). The 3D model of the deployed funnel was simplified for the simulation. Grid was generated with an element size of 25 mm, sufficiently small compared with the length scale of the deployed funnel. The simulation was conducted based on a steady-state turbulence model (SST k-epsilon) with a pressure-velocity coupling scheme set to be coupled. Fig. 9(b) represents the pressure applied on the deployed funnel at the z-x plane where y=0 m. The number of iterations was set to 200, and convergence was achieved at 144th iteration, resulting in a converged drag force of approximately 90.08 N as shown in Fig. 9(c).

3.4 Grasping force of deployable landing station

The landing station has two stable states due to the bistable structure as illustrated in Fig. 10(a), which shows the movement of flexible landing plate (red line) without arms. The grasping force of the deployable landing station depends on how strongly the arm presses the AUV, and this is determined by the restoring force of the landing plate. Thus, the force which makes the flexible landing plate buckles is analyzed using the large deflection theory and Euler beam theory (Ugural 2007, Lewis *et al.* 1981). The free-body diagram of the landing plate can be represented in Fig. 10(b). When the landing plate buckles, there is a force P that pushes the landing plate parallel to the x-axis. The curve is parameterized by its length s, with ds representing an infinitesimal displacement along the curve. The angle $\theta(s_i)$ (for $i = 1,2,\ \cdots$) between the x-axis, and the tangent to the curve at each point s_i can be used to express the differential length elements

$$dx = \cos\theta(s_i)\,ds \tag{9}$$

$$y = \sin\theta(s_i)\,ds \tag{10}$$

$$\frac{dy}{ds} = \sin\theta(s_i) \approx \theta(s_i) \tag{11}$$

When the landing plate is compressed along the x-axis, it may buckle. For any arbitrary point along the landing plate, denoted by s_i, both reaction force, R, and bending moment, M, arise. The reaction force and the bending moment at the point s are obtained through the equilibrium of forces and moments

$$R = P \tag{12}$$

$$M = EI\frac{d\theta}{ds} = -Py(s_i) \tag{13}$$

$$EI\frac{d^2\theta}{ds^2} = -P\sin\theta(s_i) \tag{14}$$

where E is Young's modulus, I is the second moment of area of the landing plate's cross section and $y(s)$ is the y-coordinate of point s. The force P according to the span of the buckled landing plate is determined by numerically solving the differential equation of Eq. (14) by using MATLAB. Then, the torque, τ, and the stored energy, U, with respect to the rotation angle of the arm, α, can be obtained

$$\tau = rP\sin\alpha \tag{15}$$

$$U = \int \tau\, d\alpha \tag{16}$$

where r is 0.05 m and maximum absolute value of α is 56° due to the given dimension of the landing station. The graph of τ and U depending on α is shown in Fig. 10(c).

The direct force, which is applied to AUV by the arms, F_{AUV}, is also calculated. When the AUV is captured, the force exerted by a single arm at the contact point with the AUV is denoted as F, which can be expressed as a function of the force P depending on α. The dimension necessary for the calculation is notated in Fig. 10(d). Given the dimensions of the designed prototype, R=0.1 m, r=0.05 m, $\gamma = 118°$, and $\alpha_{cap.} = 31°$, the other dimensions and forces can be derived

$$\beta = \pi - \alpha_{cap.} - \gamma \tag{17}$$

$$T = \frac{W}{2\ \cos(\beta)} - R\tan(\beta) \tag{18}$$

$$L = \sqrt{T^2 + r^2 - 2Tr\ \cos(\gamma)} \tag{19}$$

$$\varphi = cos^{-1}\left(\frac{T^2 + L^2 - r^2}{2TL}\right) \tag{20}$$

$$F = \frac{rP\ sin(\alpha_{cap.})}{L\ \cos(\varphi)} \tag{21}$$

$$F_{AUV} = 2F_y = 2Fcos(\beta) \tag{22}$$

Also, the location of the center of the AUV, C, is calculated as

$$C = \frac{W}{2}\tan(\beta) - \frac{R}{\cos\beta} - C_{cap.} \tag{23}$$

where the center of the captured AUV, $C_{cap.}$, is 0.0143 m. The graph of F_{AUV} depending on C is shown in Fig. 10(e) where *EI*=1 N·m². The material of the landing plate is made by layering two stainless steel plates, each with a thickness of 0.3 mm, which has a Young's modulus, *E*, of 200 GPa and a poisson's ratio, ν, of 0.27. Since the width of the landing plate, *b*, is 418 mm, the maximum direct force, which is applied to AUV by the arms, $F_{AUV.Max.}$ can be obtained by the plate theory (Landau 2012)

$$F_{AUV.Max.} = b\,D\,F_{AUV}|_{C=0} = \frac{Eh^3b}{12(1-\nu^2)}\,F_{AUV}|_{C=0} = 23.37\,N \tag{24}$$

where *D* is the flexural rigidity of the landing plate.

4. Prototype fabrication

4.1 Fabrication of deployable funnel and accessories

The primary dimensions of the prototype were determined by the constraints of the test environment. The wings, the most critical element of the deployable funnel, were designed with a length of 450 mm, which allows the funnel to achieve a maximum deployed diameter of approximately 1 m. This diameter was constrained by the 2 m width of the circulation water tunnel. Consequently, the linear actuator stroke and the dimensions of other related components were sequentially determined by these primary specifications. In the initial state, the total volume of the deployable funnel and the accessories is 1.49 m × 0.34 m ×0.20 m and the overall weight of the mechanism, including the aluminum base plate for fixture, is approximately 45 kg. In the second stage of the deployed state, the deployable funnel ascends 800 mm and reaches a diameter of 955 mm.

The deployable funnel is mainly made of nylon 12, aluminum 6061, and polycarbonate (PC). The body of the funnel is fabricated using 3D printed nylon 12, which has a density of 1.15 g/cm³. Additionally, aluminum bars are inserted into the funnel wing to enhance stiffness. The

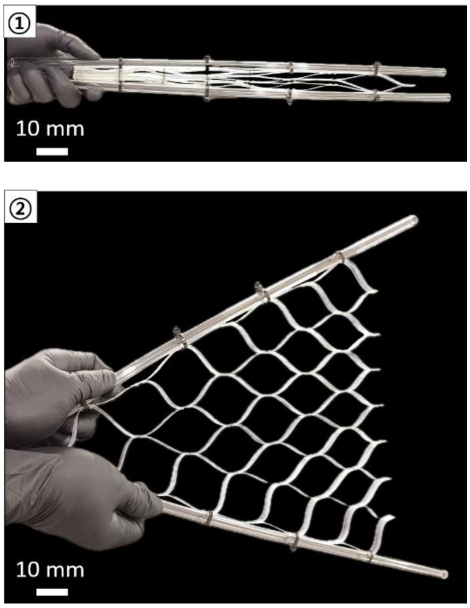

Fig. 11 The shape of the net with honeycomb structures in the initial state (①) and the deployed state (②)

actuator housing is primarily made of PC, but the parts that are prone to damage are fabricated from aluminum.

The funnel-like guide of the deployable funnel directs the AUV toward the center and subsequently constrains it by reducing the diameter of the guide. However, there is a risk of the AUV escaping through the gaps between the wings, which potentially results in collisions with the submarine. Thus, the net with a honeycomb structure, as shown in Fig. 11, is attached to cover the spaces between the wings to address the issue. It is designed to be resilient because the net without restoring force can be tangled, preventing the deployment of the mechanism. The nets are fabricated by laser cutting 1 mm thick polyethylene terephthalate glycol (PET-G) plate to provide elasticity. After that, the nets and the funnel wings are tied together.

The deployable funnel needs to be elevated far enough away from the submarine because of the wide guide area in the docking state. Therefore, the deployable manipulator is designed additionally. It uses a scissor structure, which has 1-DOF and high stowage efficiency (Liao and Krishnan 2024). It is made of PC to reduce the weight, and the

(a)

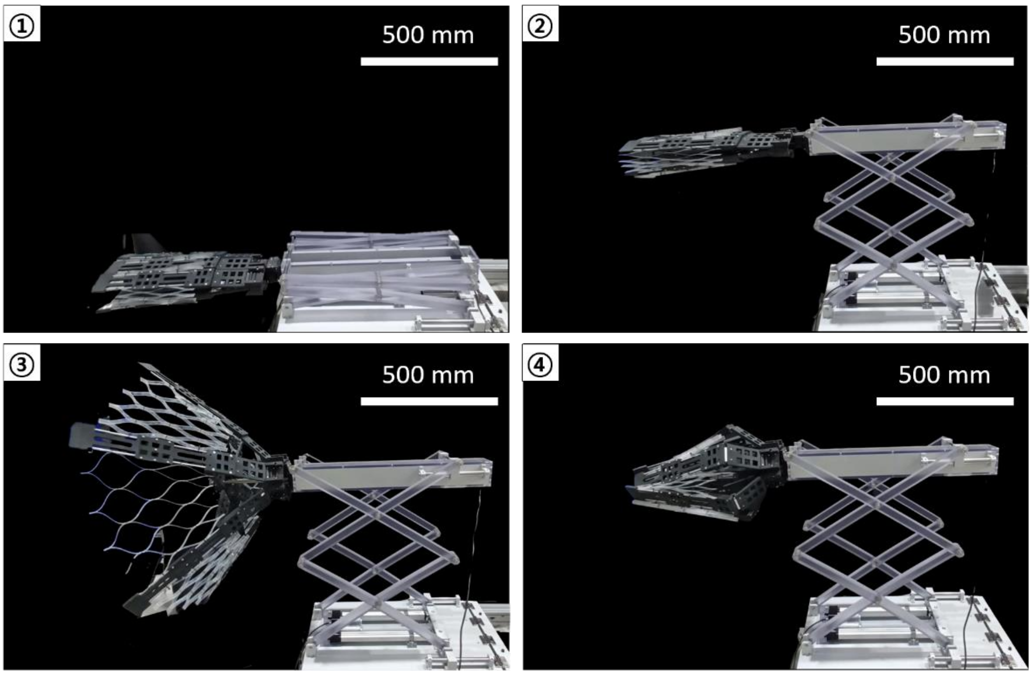

(b)

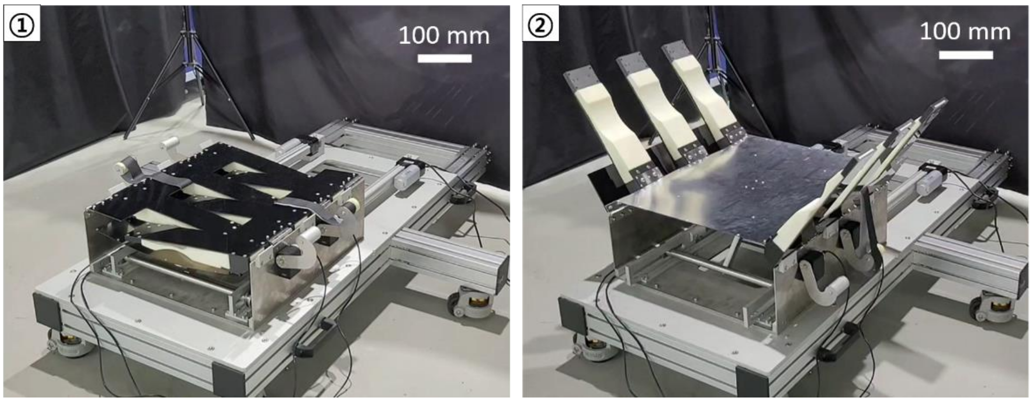

Fig. 12 Fabricated prototype (a) Deployable funnel (b) Deployable landing station

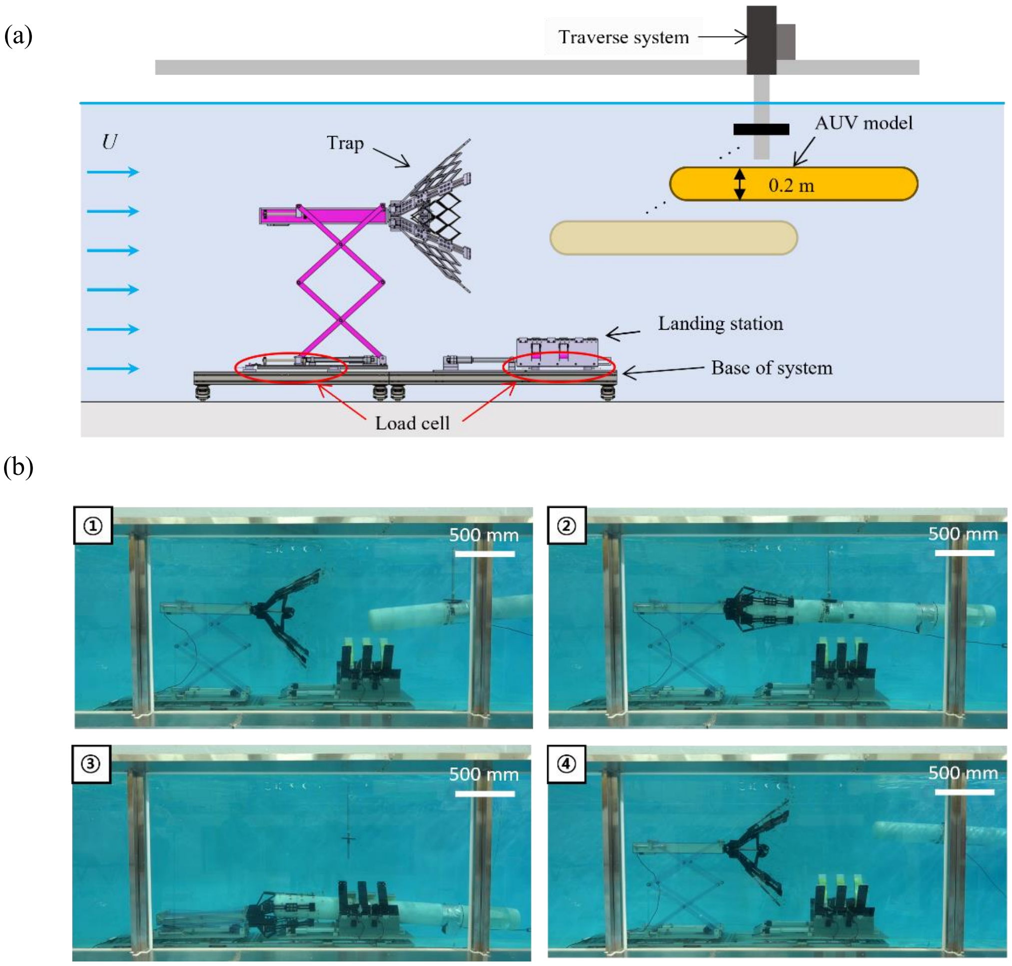

Fig. 13 (a) The configuration of the underwater experiment (b) Experiment result of the underwater docking

structural integrity was evaluated through finite element analysis (FEA) using ANSYS Workbench. The maximum stress is approximately 7.6% of the yield strength of PC, which is 60 MPa, confirming the structural safety.

The prototype of the deployable funnel for underwater docking is shown in Fig. 12(a). The mechanism was tested on the ground, which verified its reliable operation.

4.2 Fabrication of deployable landing station

The deployable landing station was designed to securely hold and guide the AUV. Considering the AUV's diameter of 200 mm and length of 2 m, the dimensions of the deployable landing station were set. As a result, the volume of the mechanism is 0.50 m × 0.48 m × 0.16 m in the initial state and the weight is about 30 kg including the aluminum base plate for fixture. In the deployed state, the guide width by the opened arms is 856 mm. This design provides sufficient width to enclose and guide the AUV, ensuring stability even when subjected to disturbances caused by water flow.

The landing station is mostly made of aluminum 6061 except the paddings, arms and landing plate. The paddings are made of polyurethane foam, which are produced using 3D printed mold to fit in the AUV shape. They are attached to arms mechanically and serve to mitigate the impact and to fasten the AUV securely by increased friction. The arms are made of PC for reliable operation through lightweight material. The landing plate is made of two 0.3 mm thick SUS304 plates that are secured with rivets to the top and bottom of the waterproof fabric. After that, it is mechanically assembled with the arms and the support pad, ensuring the synchronization of the arms' rotation angles. The prototype for underwater docking is shown in Fig. 12(b).

5. Underwater experiment

The experiment for underwater docking was conducted in a circulation water tunnel and the underwater experiment configuration is shown in Fig. 13(a). Through this experiment, the performance of the proposed system are evaluated, the drag force from the simulation and the measurement was compared, and the impact on the submarine was assessed. The AUV is towed by the traverse system but has a DOF in the x-axis direction. So, the deployable funnel can drag the AUV down to be fixed by the deployable landing station. The result of the underwater docking is shown in Fig. 13(b), which verifies secure constraint of the AUV. The variation of the forces, which is exerted downward by the system, was measured using eight

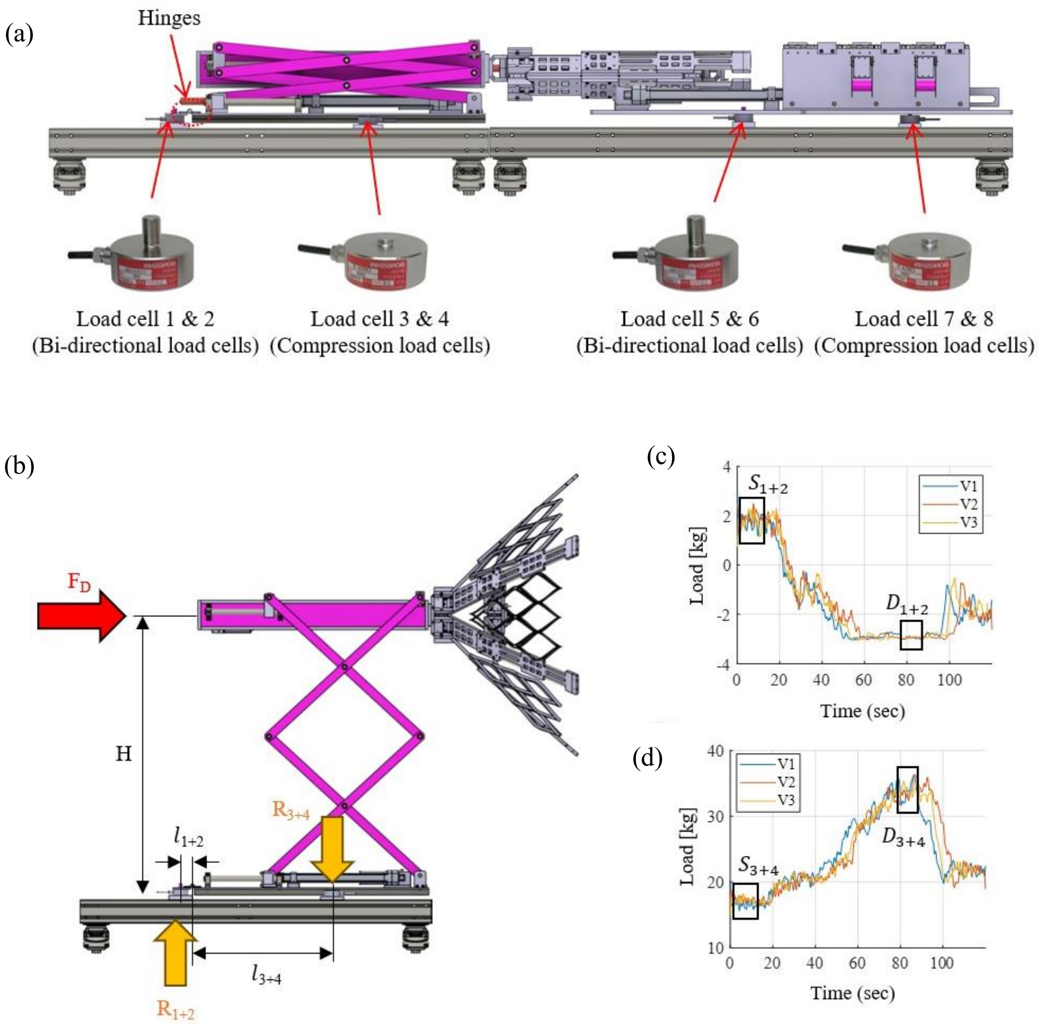

Fig. 14 (a) Position of the load cells (b) Free body diagram of the fully deployed funnel (c) Measured loads on load cells 1 and 2 (d) Measured loads on load cells 3 and 4

single-axis load cells. There are two types of load cells, CBESA (compression load cells) and CDES (bi-directional load cells) series, made by BONGSHIN LOADCELL. As shown in Fig. 14(a), four load cells are positioned beneath the deployable funnel and the others are placed beneath the deployable landing station symmetrically.

When the funnel is fully deployed, it is expected to undergo significant drag force due to dynamic pressure and shear stress around its wings, which are spread over a large area in a funnel-like shape. Therefore, the base of the system was designed to analyze fluid resistance through calculating moments. Specifically, load cells 1 and 2, which are near the inflow of water, are capable of sensing both tension and compression. Also, the plate above load cells 1 and 2 is hinged to the plate above load cells 3 and 4, enabling the measurement of the force applied to the funnel.

The effect of fluid on the funnel was measured three times, and the average was used for calculation. For the load cell measurements, the data presented were filtered using a 5th-order Butterworth low-pass filter. The sampling frequency was 25 Hz, and the cutoff frequency was set to 1 Hz. Fig. 14(b) depicts the free body diagram of the fully deployed funnel. Fig. 14(c) and Fig. 14(d) show the changes in loads on load cells 1-4 from the initial state with the folded manipulator to the docking state with the deployed manipulator. S_{1+2} and S_{3+4} represent the average of the measured loads in the initial state, while D_{1+2} and D_{3+4} represent the average of the measured loads in the fully deployed state. The legends V1, V2, and V3 correspond to the first, second, and third measurements, respectively. Then, the reaction forces at the centers of load cells 1 and 2, and 3 and 4 can be obtained

$$\boldsymbol{R}_{\boldsymbol{1+2}} = |S_{1+2} - D_{1+2}| \times 9.8\, m/s^2 = 46.06\, N \tag{25}$$

$$\boldsymbol{R}_{\boldsymbol{3+4}} = |S_{3+4} - D_{3+4}| \times 9.8\, m/s^2 = 106.81\, N \tag{26}$$

where the values of S_{1+2}, D_{1+2}, S_{3+4}, D_{3+4} are 1.798 kg, -2.935 kg, 17.114 kg, 33.524 kg, respectively. The drag force applied to the funnel by fluid, F_D, can be calculated through the equilibrium of moments

$$R_{1+2} \times l_{1+2} + R_{3+4} \times l_{3+4} = H \times F_D \tag{27}$$

The force F_D is 98.79 N where the values of l_{1+2}, l_{3+4}, H are 0.04 m, 0.48 m, 0.8 m, respectively (the value obtained from the CFD simulation is 90.08 N).

The impact on the submarine is assessed by measuring

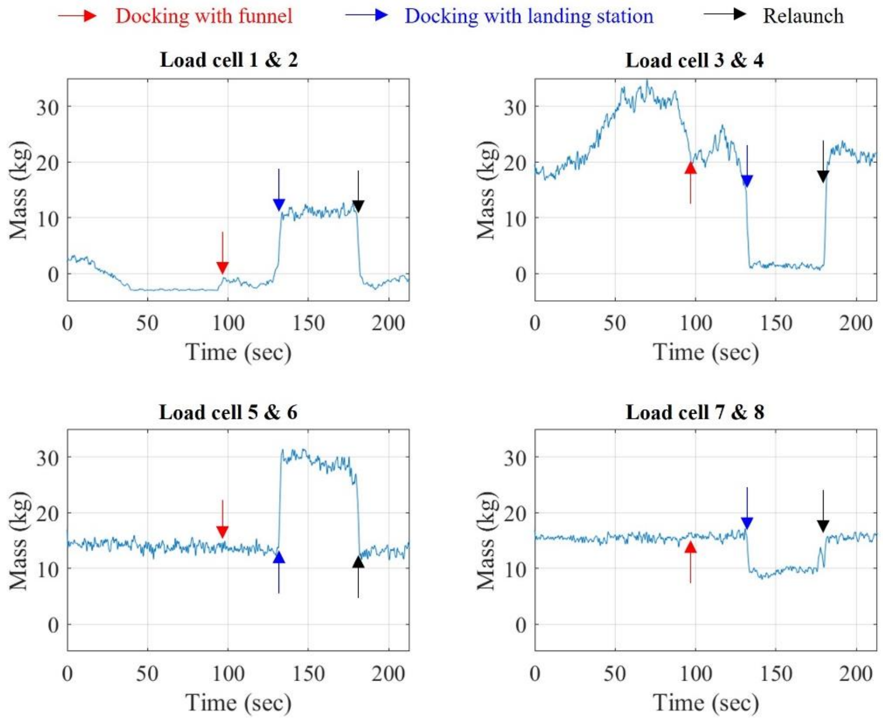

Fig. 15 Measured loads on load cells 1–8 during the entire docking process

the loads during the entire docking process. Fig. 15 shows that the water flow exerts pressure on the deployable funnel significantly as previously analyzed. On the other hand, the effect of the water flow on the deployable landing station is insignificant because the cross-sectional area in the x-y plane is small. After the AUV docking is completed, the downward force from the funnel has a major influence on the distribution of loads. But this variance decreases by elevating the deployable funnel.

6. Discussion

In this paper, a transformable underwater docking system is presented, which enables a submarine to recover the AUV directly. The system is divided into deployable funnel and deployable landing station for initial capture, and stabilization of the AUV, respectively. First, the deployable funnel captures the AUV and drags it down to the deployable landing station. After that, the deployable landing station fastens the AUV for charging and data transmission. They are folded into a flat configuration with a height of less than 0.2 m. When they are deployed, the funnel-like guide of the deployable funnel has a diameter of 0.955 m, and the guide of the deployable landing station has a width of 0.856 m. Therefore, the proposed mechanism can perform docking stably, while it can be stowed in the submarine compactly.

The performance of the mechanism was verified by underwater experiments in the circulation water tunnel with a free-stream velocity U=0.6 m/s and the system reliability, including impacts on the host submarine, are evaluated through the measurement by load cells. Further work will focus on a more detailed fluid dynamics analysis. A comprehensive CFD or particle image velocimetry (PIV) analysis is planned to validate the deployable funnel's performance under various flow conditions.

In the underwater experiment, the AUV model was towed by the traverse when it was approaching the docking mechanism because fully autonomous operation of an AUV within a confined water tank environment has significant challenges due to spatial constraints, and sensor limitations. Moreover, such automation is considered beyond the scope of this study, which primarily focuses on the mechanical design and validation of the docking mechanism. The performance of the mechanism was verified sufficiently whether the AUV model could be reliably recovered and launched. Although fully autonomous operation was not implemented in this work, the potential for automated recovery will be further researched by integrating waterproof contact sensors.

Material selections can be improved to suit harsh marine environments in future work. The grasping performance of the deployable funnel can be enhanced by improving friction between the funnel surface and the AUV through the integration of high-friction materials such as polyurethane or specialized marine-grade elastomers. Surface patterning techniques can also be applied to further increase friction coefficients. Additionally, the current PET net structure between funnel wings presents durability limitations while offering sufficient flexibility. Thus, this material could potentially be replaced with other synthetic fibers that have enhanced stiffness to ensure sustained operational performance (Pour *et al*. 2024).

The proposed mechanism is also applicable to various docking environments that require compatibility between various platforms, space efficiency, and compensation for misalignments. For instance, it can enable reliable docking between aircraft for aerial refueling, and modular robots for rapid moving in cluttered environments. This flexibility improves operational efficiency and offers a practical solution for various docking systems.

Acknowledgements

This research was supported by the Challengeable Future Defense Technology Research and Development Program through the Agency for Defense Development (ADD) funded by the Defense Acquisition Program Administration (DAPA) in 2024 (No.915071101).

References

Cha, J.H., Noh, J.S., Sathish Kumar, S.K., Jin, D., Lee, D.Y. and Kim, C.G. (2024), "Origami multi-layer space shield for cylindrical space structure", *Chin. J. Aeronaut.*, **37**, 294-312. https://doi.org/10.1016/j.cja.2024.06.004.

Esteba, J., Cieślak, P., Palomeras, N. and Ridao, P. (2024), "Sparus docking station: A current aware docking station system for a non-holonomic AUV", *J. Field Robot.*, **41**(6), 1765-1779. https://doi.org/10.1002/rob.22310.

Fedor, R. (2009), "Simulation of a launch and recovery of an UUV to a submarine", KTH Royal Institute of Technology, Sweden.

Guevara-Corzo, J.J., Begambre-Carrillo, O.J., Garcia-Sanchez, J.A. and Sanchez-Acevedo, H.G. (2022), "Passive seismic protection systems with mechanical metamaterials: A current review", *Struct. Eng. Mech.*, **82**(4), 417-434. https://doi.org/10.12989/sem.2022.82.4.417.

Guo, J., Liu, M., Pan, X., Zhu, J., Liu, J., Xu, H., Peng, Z. and Cui, J.H. (2024a), "Moored underwater docking system for resident UUVs with acoustic guidance: Design and experiment", *Ocean Eng.*, **294**, 116802. https://doi.org/10.1016/j.oceaneng.2024.116802.

Guo, J., Tan, H., Liu, J., Feng, W., Peng, Z., Liu, Y. and Cui, J. H. (2024b), "Numerical simulation and analysis of UUV docking with a seabed moored floating dock", *Ocean Eng.*, **313**, 119528. https://doi.org/10.1016/j.oceaneng.2024.119528.

Hwang, Y.H. and Han, J.H. (2025), "Crashworthiness of energy absorbing structures under combined shear-compression loading: Effects of materials and geometries", *Int. J. Aeronaut. Space Sci.*, **26**, 615-628. https://doi.org/10.1007/s42405-024-00779-5.

Kim, T.H., Lee, D.Y. and Han, J.H. (2025), "Construction of metre-scale foldable space shelter based on gravity-driven self-assembling origami", *Scientif. Report.*, **15**, 19615. https://doi.org/10.1038/s41598-025-04241-8.

Koetsier, T. and Ceccarelli, M. (2012), *Explorations in the History of Machines and Mechanisms*, Proceedings of HMM2012, Vol. 15, Springer Science & Business Media.

Lewis, G. and Monasa, F. (1981), "Large deflections of cantilever beams of nonlinear materials", *Comput. Struct.*, **14**(5-6), 357-360. https://doi.org/10.1016/0045-7949(81)90054-7.

Li, J., Cong, Q. and Chen, T. (2025), "Design and study of a bionic docking device for autonomous underwater vehicles", *Ocean Eng.*, **328**, 121041. https://doi.org/10.1016/j.oceaneng.2025.121041.

Liao, Y. and Krishnan, S. (2024), "Deployable scissor structures: Classification of modifications and applications", *Auto. Constr.*, **165**, 105547.

Lin, M., Lin, R., Yang, C., Li, D., Zhang, Z., Zhao, Y. and Ding, W. (2022), "Docking to an underwater suspended charging station: Systematic design and experimental tests", *Ocean Eng.*, **249**, 110766. https://doi.org/10.1016/j.oceaneng.2022.110766.

Martin, S., Fletcher, B., Flores, G., Jones, A., Nguyen, A., Caruso, N. and Brown, M.H. (2016), "Characterizing the critical parameters for docking unmanned underwater vehicles", *OCEANS 2016 MTS/IEEE Monterey*, 1-7.

Misseroni, D., Pratapa, P.P., Liu, K., Kresling, B., Chen, Y., Daraio, C. and Paulino, G.H. (2024), "Origami engineering", *Nat. Rev. Meth. Prim.*, **4**(1), 40. https://doi.org/10.1038/s43586-024-00313-7.

Morris, C.G. (1992), *Academic Press Dictionary of Science and Technology*, Gulf Professional Publishing.

Park, G., Yang, D.W., Oh, M.W., Chae, J.S., Yoon, H., Han, J.H. and Lee, D.Y. (2025), "Deployable mesh reflector antenna for global navigation satellite system radio occultation within 1U CubeSat form factor", *Aerosp. Sci. Technol.*, 110694. https://doi.org/10.1016/j.ast.2025.110694.

Pour, A.K., Shirkhani, A. and Farsangi, E.N. (2024), "Spalling resistance and mechanical performance of UHPC under high temperature using hybrid natural and artificial fibers", *Struct. Eng. Mech.*, **91**(2), 177-195. https://doi.org/10.12989/sem.2024.91.2.177.

Tian, A., Zhang, L., Liu, J., Shao, S., Zheng, J., Xu, N., Chen, Z. and Hanif, M. (2024), "Design, optimization and verification of a conical guiding origami mechanism for underwater docking station", *Ocean Eng.*, **298**. 117205. https://doi.org/10.1016/j.oceaneng.2024.117205.

Ugural, A.C. (2007), *Mechanics of Materials*, John Wiley & Sons.

Waldron, K.J., Kinzel, G.L. and Agrawal, S.K. (2016), *Kinematics, Dynamics, and Design of Machinery*, John Wiley & Sons.

Wu, Y., Zheng, N., Wu, Y. and Yang, Q. (2024), "Electric field strength effect on bi-stability of composite thin cylindrical shell with piezoelectric layer", *Struct. Eng. Mech.*, **89**(6), 571-578. https://doi.org/10.12989/sem.2024.89.6.571.

Zhang, T., Li, D. and Yang, C. (2017), "Study on impact process of AUV underwater docking with a cone-shaped dock", *Ocean Eng.*, **130**, 176-187. https://doi.org/10.1016/j.oceaneng.2016.12.002.

Zhang, W., Wu, W., Teng, Y., Li, Z. and Yan, Z. (2023), "An underwater docking system based on UUV and recovery mother ship: design and experiment", *Ocean Eng.*, **281**, 114767. https://doi.org/10.1016/j.oceaneng.2023.114767.

CC